The MorphoColor Concept for Colored Photovoltaic Modules

Benedikt Bläsi, Thomas Kroyer, Tilmann E. Kuhn, and Oliver Höhn

***Abstract*—We introduce a photonic color concept for integrated photovoltaic modules. Taking up the inspiration from the Morpho butterfly with its brightly colored wings, we developed this photonic concept further to achieve an improved angular independent color effect, suitability for module integration, and compatibility with industrial production processes, while maintaining high module efficiencies. We demonstrate the steps that lead to the optimized photonic structure and explain the underlying optical effects. Using the data from demonstrator modules, we show the outstanding performance in terms of module efficiency and color stability. A power output for the MorphoColor modules of more than 94% compared to the reference module power is shown.**

***Index Terms*—Biomimetics, building integrated photovoltaics (PVs), color filters, photon management, photonic structure, PV modules.**

I. Introduction

COLORED photovoltaic (PV) modules are an interesting option to support acceptance and attractivity of building integrated PV (BIPV). Especially architects, building planners, and building owners desire an individual color choice, saturated colors, a homogeneous appearance for all angles of incidence, and viewing directions and at the same time, a high module efficiency. Furthermore, glare should be suppressed.

Since there is a very large variety of color concept for BIPV, it would be beyond the scope of this introduction to give a comprehensive list. For an overview of approaches, we refer to recent review papers [1], [2]. Still, we give some important examples in order to show the possibilities and limits of state-of-the-art technologies.

One possibility to achieve a colorful appearance is the use of colored PV cells. With organic PVs [3], Perovskite [4], and dye sensitized solar cells [5], material-intrinsic coloring is possible. However, the disadvantages are e.g., relatively low efficiency compared to silicon, a short lifetime, and a very limited color selection. When adapting the cell surface (e.g., the antireflective coating for Si) or the layer structure (for CIGS, CdTe, and thin-film Si), the possible color range is severely limited, the reflection losses are very high (significantly higher than 10%), the angular stability of the color is poor, and industrial implementation is costly due to intervention in the cell production process. In addition, the cells are still recognizable as such in the module [6].

To achieve aesthetic photovoltaic building skins, one approach is to use a decorative module component in front of the solar cell layer. Colored encapsulants or printed glass covers suffer from low color saturation or high power loss relative to a conventional module [7]. One concept is the use of diffusing foils in light colors with low color saturation as well as in white. However, the high degree of scattering reflection leads to significant losses in efficiency (25–50%) [8]. An option to mitigate such losses is the use of luminescent materials [9], leading to only small reductions in electrical power or even a slight enhancement, if the spectral response on the used solar cell is weak in the absorption range of the luminescent dye.

Another concept is to use specially adapted interference coatings on planar glass substrates. However, the color range is limited to pastel shades, and colors with high angular stability and saturation can hardly be realized in this way. Due to the very different layer structure for each color, flexible production of different color variants is difficult [10], [11].

In summary, state-of-the-art concepts offer a restricted choice of colors, show a strong angular dependence, cause a high efficiency loss or do not allow for an efficient industrial production. We overcome these restrictions by the MorphoColor approach [12] inspired by the Morpho butterfly effect [13], [14]. The complex 3-D photonic structures found in nature feature highly saturated colors with low angular dependence. In this article, we go beyond this bionic concept to achieve high transmission, improved color saturation and angular stability, suitability for PV module integration, and compatibility with industrial production processes.

II. Adapting the Morpho Effect

A. The Morpho Butterfly Effect

The Morpho butterfly features a delicate 3-D photonic structure consisting of ridges and lamellae attached to them [13], [14]. Kinoshita *et al.* [15], [16] described the effect using a basic model consisting of infinitely thin and equally spaced lamellae in air, which cause a Bragg reflection effect. Furthermore, the lamellae have a limited width and a (randomly distributed) vertical offset to the neighboring lamellae stack. The latter features cause diffraction, resulting in an angular distribution.

Manuscript received March 15, 2021; revised May 20, 2021; accepted June 7, 2021. Date of publication July 5, 2021; date of current version August 20, 2021. This work was supported by the German Federal Ministry of Economic Affairs and Energy under Contact 03EE1049A (PV-Hide) and Contact 03ETW007A (Farbkollektor). *(Corresponding author: Benedikt Bläsi.)*

The authors are with the Fraunhofer Institute for Solar Energy Systems ISE, 79110 Freiburg, Germany (e-mail: benedikt.blaesi@ise.fraunhofer.de; thomas.kroyer@ise.fraunhofer.de; tilmann.kuhn@ise.fraunhofer.de; oliver.hoehn@ise.fraunhofer.de).

Color versions of one or more figures in this article are available at https://doi.org/10.1109/JPHOTOV.2021.3090158.

Digital Object Identifier 10.1109/JPHOTOV.2021.3090158

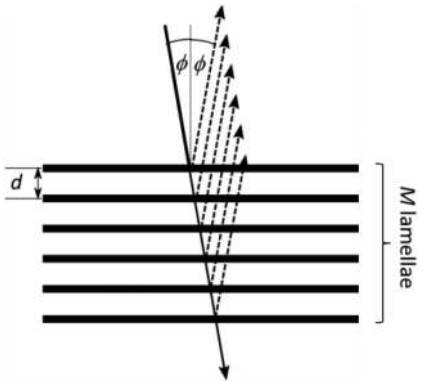

Fig 1. "Simple Bragg model" with angle ϕ, distance d, and lamellae number M.

In order to better understand the effect of the lamellae, we focus our investigation on the Bragg term, or, more generally, the thin film effect. With the angle of incidence (equaling the reflected angle) ϕ, the Bragg term in [16] is as follows:

$$I_\phi \sim \frac{\sin^2(kd\nu M/2)}{\sin^2(kd\nu/2)}$$

with $k = 2\pi/\lambda$, λ the wavelength, d the distance between lamellae, $\nu = 2\cos(\phi)$, and M the number of lamellae (see also Fig. 1). We call this the "simple Bragg model," which has already been used for describing x-ray diffraction in 1913 [17].

B. Harmonics in the Simple Bragg Model

The color observed at the Morpho butterfly is caused by lamellae, which have a distance $d = \lambda_0/2$, where λ_0 is the design wavelength, i.e., the wavelength at the center of the reflectance peak. We call this the 0th harmonic configuration. Of course, a reflectance peak at λ_0 can also be caused by higher harmonic configurations: First harmonic with $d = \lambda_0$, Second harmonic with $d = 3\lambda_0/2$, etc.

If we compare the resulting reflectance spectrum of the configurations with the 0th (black line) or the 2nd (red line) harmonic reflectance peak located at $\lambda_0 = 550$ nm, we can see that the peak at λ_0 is narrower for the 2nd harmonic (see Fig 2). Such a narrower peak has two advantages for the desired BIPV application: a higher spectral transmittance (i.e., lower efficiency loss) and a higher color saturation. However, this comes at the price of two additional peaks within the spectral range that is relevant for silicon PV: one at 825 nm (1st harmonic) and one at 412.5 nm (3rd harmonic). In a PV module, both reflectance peaks would causelosses and a color shift.

C. Harmonics in the Thin Film Model

At this point, it is important to note that the simple Bragg model does not describe the system correctly, since it assumes infinitely thin lamellae. Therefore, this model is refined by using a Bragg stack consisting of four layers with thickness $\lambda_0/4n$ (or $3\lambda_0/4n$ for the 2nd harmonic configuration) and a refractive index of $n = 1.5$, spaced by air gaps of width $\lambda_0/4$ (or $3\lambda_0/4n$). The two systems are depicted in Fig 3.

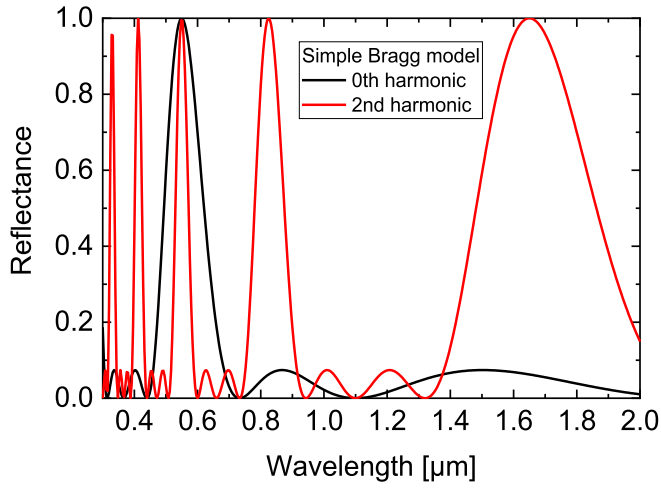

Fig 2. Reflectance spectra calculated with the simple Bragg model for four lamellae in air with $\lambda_0 = 550$ nm.

Fig 3. Left: thin lamella system described by the simple Bragg model. Right: Bragg stack consisting of four layers with defined thickness.

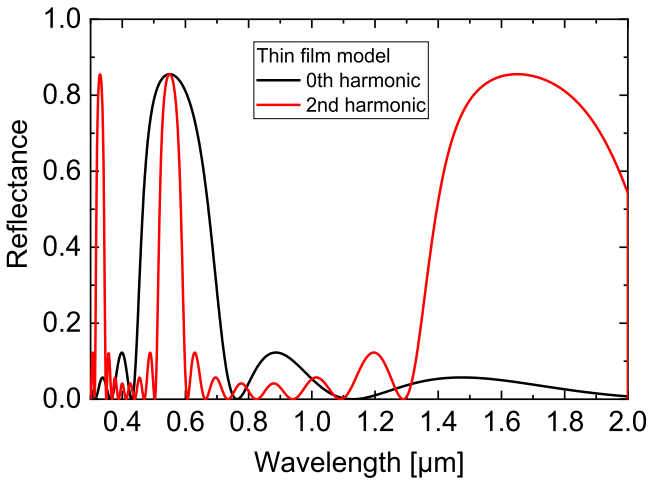

Fig. 4. Reflectance spectra for four $\lambda_0/4n$ thick lamellae in air, calculated with the TMM ($\lambda_0 = 550$ nm).

The system is simulated using the transfer matrix method (TMM) [18]. With this model, we can reproduce the impact of the harmonic on the peak width at $\lambda_0 = 550$ nm. However, for the 2nd harmonic configuration, the 1st and 3rd harmonic peaks vanish (see Fig. 4). This is due to destructive interference of partial waves reflected from the top and bottom interfaces of the lamellae. To understand this effect, we take a closer look at a single lamella. In the 0th harmonic configuration, it has anoptical thickness of $\lambda_0/4$. The optical path difference

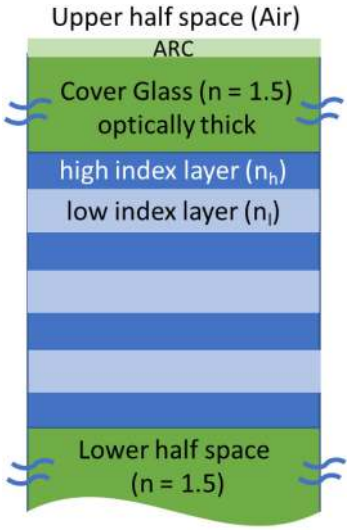

Fig 5. Definition of the general model system and materials for module integration.

of two waves reflected at top and bottom of the lamella is $\lambda_0/2$. Together with the phase shift of π for the partial wave reflected at the top of the lamella, the resulting phase difference is 0, leading to constructive interference. This is also true for the 2nd, 4th, … harmonic configurations with optical lamella thicknesses of $3\lambda_0/4$, $5\lambda_0/4$, …. However, for the 1st, 3rd, 5th, … harmonic configuration, the optical lamella thicknesses are $\lambda_0/2$, λ_0, $3\lambda_0/2$, …, leading to optical path differences of λ_0, $2\lambda_0$, $3\lambda_0$, …. Together with the phase shift of π, this leads to an overall phase difference of $3\pi, 5\pi, 7\pi$, … resulting in vanishing peaks for these harmonics.

D. Module Integration, Refractive Index, and Angular Dependence

Lamellae suspended in air are not a realistic structure for the use in a PV system. As the Morpho structure shall be integrated at the interface between the cover glass and the encapsulant, more materials and interfaces need to be considered. Therefore, we first define the modeled system and the relevant materials (see Fig 5). The thin film stack consists of high index layers (n_h) and low index layers (n_l). Above this stack, the cover glass is represented by an optically thick absorption free superstrate with $n = 1.5$. The medium from which the light enters the system (upper half space) is air. This implies that angles of incidence are defined in air. In order to suppress front side reflection effects, an antireflection coating (ARC) with $n = 1.25$ (representing to a nanoporous SiO_2 layer) and thickness 130 nm is applied. Finally, the lower half space with $n = 1.5$ represents the encapsulant in which the light is transmitted.

To adapt the system described in the last section to the integrated situation, the refractive indices are chosen to be $n_h = 2.0$ and $n_l = 1.5$. Again, four high index layers with thickness $3\lambda_0/4n_h$ are spaced by low index layers with thickness $3\lambda_0/4n_l$ (2nd harmonic configuration). This system will be referred to as "$n = 2.0/1.5$."

At normal incidence, this system shows a very similar behavior as the 2nd harmonic system in the last section (see Fig. 6).

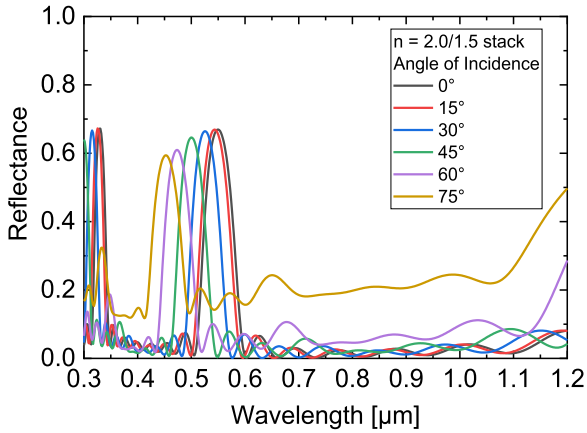

Fig. 6. Angle dependent reflectance spectra for the module integrated $n = 2.0/1.5$ stack.

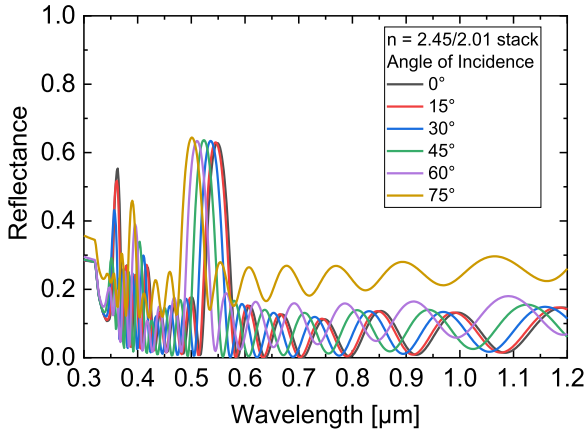

Fig. 7. Angle dependent reflectance spectra for the module integrated $n = 2.45/2.01$ stack.

With increasing angle of incidence, we observe the characteristic shift of the peak toward shorter wavelengths (blue shift).

As a next step, the refractive index of the thin films is further increased, and real data of sputter coated materials are used: The high index material is TiO_2 ($n_h = 2.45$ @ 550 nm) and the low index material is SiN ($n_l = 2.01$ @ 550 nm). The wavelength dependent n and k data can be found in Appendix A Fig. 14. Apart from this, the stack is unchanged. The reflectance spectra of this modified "$n = 2.45/2.01$" system are shown in Fig. 7.

Two effects of this change can be seen: The reflectance peak gets narrower, reducing the full width at half maximum (FWHM) at normal incidence from 60 to 43 nm. Furthermore, the incidence angle dependent shift of the peak position is reduced from 97 nm (between normal and 75° angle of incidence) to 47 nm. This translates to improved color stability. As a general design rule, high refractive indices in the layer stack and the use of higher harmonics (only even numbers) lead to narrower peaks and an improved color stability.

E. Optimization for Efficient Industrial Production

The $n = 2.45/2.01$ system still shows properties that are not ideal in terms of optical performance and industrial production: The reflectance spectra show strong oscillations in the spectral ranges where, low reflectance is desired. Furthermore, the thin

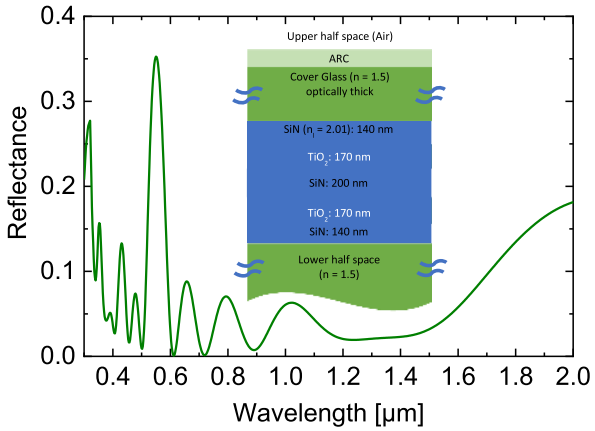

Fig. 8. Reflectance spectrum of the optimized thin film stack.

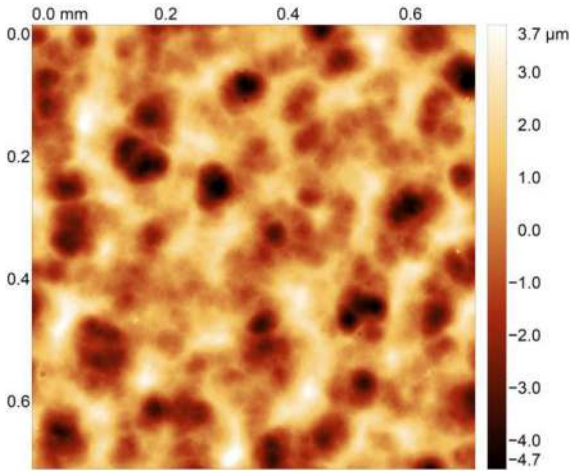

Fig. 9. Confocal microscopy image of the etched glass surface.

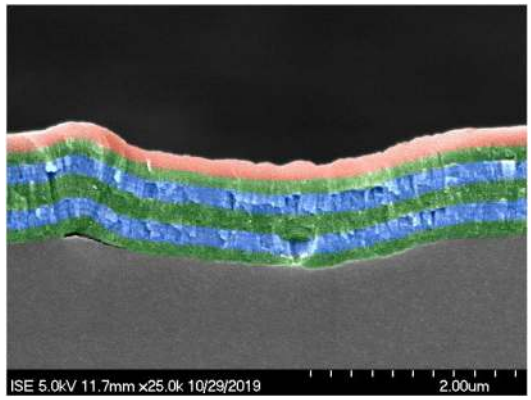

Fig. 10. SEM cross section of the layer stack deposited on the etched glass surface. The layer materials are indicated by false colors: green for SiN, blue for TiO_2, and coral for SiO_2. The SiO_2 layer is index matched to the encapsulant and has no optical function in the module.

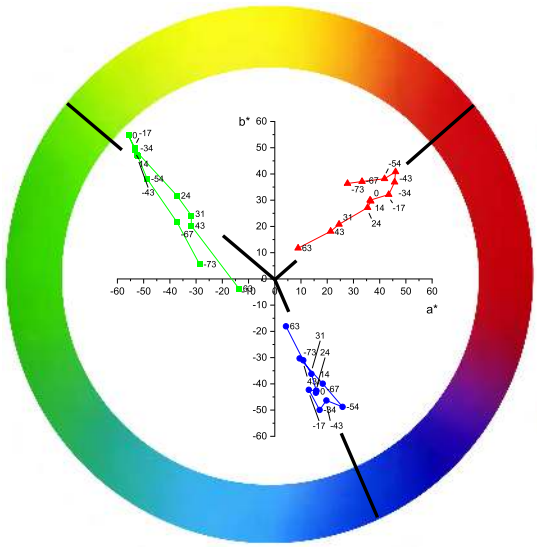

Fig. 11. Representation of the data extracted from the angle dependent photographs for the green, blue, and red modules in the a^*b^* plane, showing the color stability. The main hue directions are indicated by black lines.

film layer stack is rather thick (1287 nm), which would require a long deposition time and high production cost. To give an example, the deposition time on a PVD lab coater is about 3h for the layout with four high index layers.

As a further optimization, the stack was reduced from 4 to 2 high index layers, reducing the deposition time to appr. 50%. With optimized coating processes using industrial production equipment, this can be substantially reduced. Furthermore, additional low index layers at the transition to the $n = 1.5$ material were introduced in order to reduce the unwanted oscillations. With these measures, the overall thickness of the thin film stack is reduced to 820 nm. The resulting reflectance spectrum is shown in Fig. 8.

Due to the smaller number of high index layers, the reflectance peak is lower, resulting in a somewhat lower color brightness. The lower peak in combination with the low index layers at the edges to suppress side oscillations result in reduced reflection losses.

F. Combination of Thin Films and Structured Surface

So far, we focused the investigation on the thin film aspect of the Morpho effect. However, for the full Morpho effect, the angular distribution is a crucial component. In nature, this is achieved by a limited lamella width and a (randomly distributed) height difference to the neighboring lamellae stack. Chung *et al.* [19] showed that the Morpho effect can also be reproduced by depositing a Bragg stack onto a structured surface, resulting in a 3-D photonic structure consisting of stacked corrugated layers. Taking up this idea, we applied the optimized stack described in the previous section to a structured glass surface [20] and used it as cover glass for a PV module [12], [21]. In a first screening of suitable structures for industrial production, we identified glass textured in a hexafluoric acid based etch solution as a good option. The topography, measured by confocal microscopy (3-D Laser Microscope LEXT OLS4000, Olympus), is shown in Fig. 9. The typical lateral feature size (extracted from the radial autocorrelation function using the software Gwyddion [22]) is 30 μm, and the rms roughness is 1.5 μm. The surface inclination angles are below 25°, with a major part below 10° (average slope

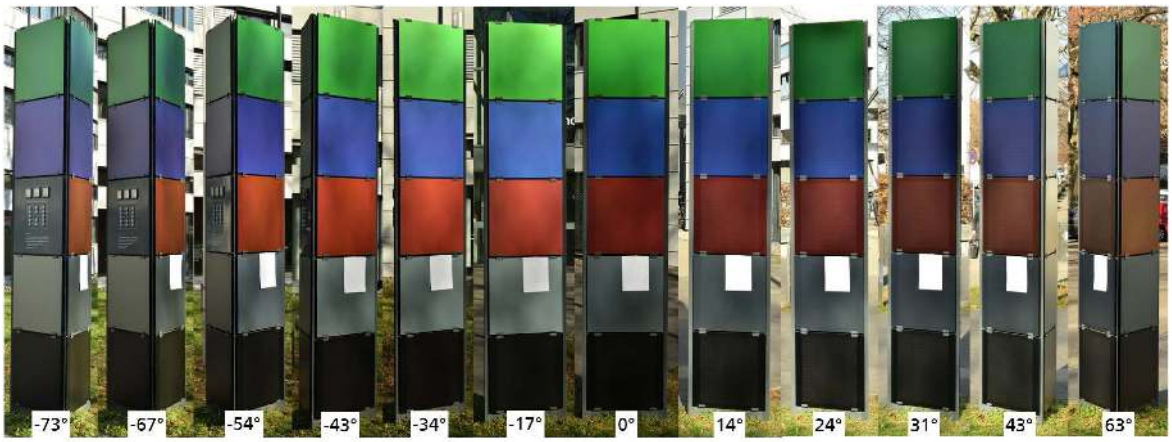

Fig. 12. Series of photographs of the stele with demonstrator modules, taken from 12 different azimuth angles (73° left to 63° right).

Fig. 13. Demonstrator modules of the format $1.0 \times 1.0\ m^2$. Slight changes in color close to the edges are caused by deposition rate variations in the lab coater.

angle: 6.7°). A cross section of the thin films on the texture is shown in Fig. 10.

A detailed investigation of the photonic interactions between structure and thin film stack is the focus of ongoing research. First results indicate that the slope angle distribution is a very important parameter. Too small inclinations result in a reduced angular stability, while too steep slopes reduce the homogeneity of the layer stack.

While the model systems shown so far were optimized for the color green (with a reflectance peak centered at 550 nm), the effect is not restricted to this color. With a scaling of all the thicknesses, other peak wavelengths can be chosen and, hence, other colors created.

Taking all the processes together, the estimated production cost for adding the MorphoColor concept is 30–100 €/m^2 [7]. Since this is still a technology under development, this can only be a rough estimate, to be further specified as the processes are transferred to industrial production.

III. Morpho Color Module Results

As a demonstrator, modules with the colors green, blue, red, and grey were produced together with a black reference module without MorphoColor interface. At the front side of the cover glass, an additional antiglare structure is applied. The modules have the format $0.6 \times 0.6\ m^2$. The solar cells within the modules are shingled monocrystalline siliconPERC type cells (TW Solar M1565BPERC 156.75, Tongwei Solar), which show a very homogeneous appearance and are therefore very well suited for integrated PV systems [23]. They are installed in a stele in front of the Fraunhofer ISE main building in Freiburg, Germany.

Fig. 12 shows a series of photographs of this stele, taken from different angles (73° left to 63° right) on 18th November 2020, 1 pm. The solar elevation angle was 22°, the azimuth angle 20° to the right of the surface normal. Even if it was a sunny day with a large fraction of direct sunlight, the modules are partly shaded by trees.

From the camera (Nikon D3300), the image raw RGB data were taken, the paper sheet at the bottom used for the white balance, and $L^*a^*b^*$ color coordinates [24] calculated from the balanced RGB values (details in Appendix B). In this coordinate system, L^* is the lightness (values from 0 to 100), and a^* and b^* express the color in terms of hue (direction in the color wheel) and chroma (distance from the origin). This means that points with a large distance from the origin represent highly saturated colors. Even if this is not an exact measurement as it would be obtained by using a luminance camera, the results demonstrate the excellent color stability. In Fig. 11, the values for the green, blue, and red modules are displayed in the a^*b^* plane. The main hue directions are indicated by black lines. From this plot, we can see that the colors are less saturated (points closer to the origin) toward larger angles. This can be understood from the increased overall reflectance for larger angles. Furthermore, the angle dependent small shift of the reflectance peak leads to a small counter clockwise color shift toward orange (for red) and toward turquoise (for green) for large angles. For the blue color, no systematic angle dependent hue change larger than the uncertainty of the values can be observed.

We observe a very similar behavior if the sun is lower in the sky and the incident spectrum is shifted toward longer wavelengths. Of course, the reflected spectrum is changed, but this also applies to the white point, resulting in a very similar color perception. Under diffuse illumination (cloudy sky), the angular stability is even better.

In order to demonstrate the compatibility of the technology with large-scale production, modules of the format $1.0 \times 1.0\ m^2$ were manufactured externally using an array of 7×7 back

TABLE I
MODULE PERFORMANCE (DATA FROM [25]).

Module	reference	blue	green	red
P_{mpp} [W]	155.2	146.5	146.4	146.7
relative to reference		94.4%	94.3%	94.5%

contact cells from Sunpower Corp. with a black back sheet in order to achieve a homogeneous appearance (see Fig. 13).

The performance of the MorphoColor modules was measured at Fraunhofer ISE CalLab PV Modules and compared to a reference module without photonic structure [25]. All modules have an antiglare structure at the front. The power values are listed in Table I. The measurements demonstrate that the MorphoColor structures lead to a very small loss and a power of $> 94\%$ compared to the reference can be achieved.

IV. CONCLUSION

We showed how the Morpho structure as found in nature can be modified in order to feature an enhanced color saturation and stability, while at the same time transmitting a large fraction of the incident solar radiation to the solar cells within a PV module. In addition to these performance improvements, the combination of the adapted thin film stack with a surface structure is well suited for industrial production.

Beyond the design and proof of concept, we demonstrated color effects and PV performance of test modules, resulting in more than 94% power compared to a black reference module.

This will help integrating high efficiency PV modules into buildings, but also into other applications such as vehicles, tapping the very large potential of integrated PV.

While we focused on PV modules in this article, the MorphoColor concept can also be applied to solar thermal collectors, enabling a better building integration, leading to an improved acceptance and an increased deployment of integrated solar systems.

APPENDIX

A. Measured Refractive Index Data of TiO_2 and SiN

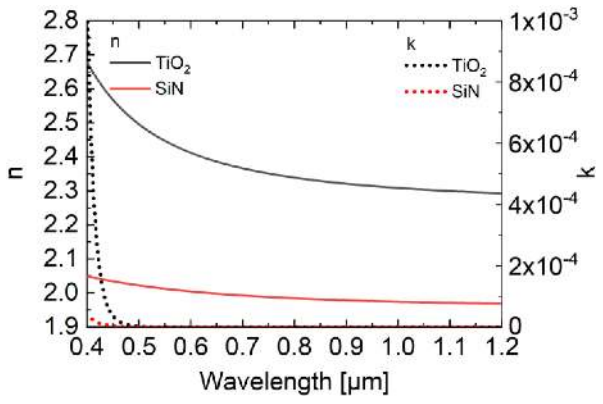

Fig. 14. n and k values of the used TiO_2 and SiN materials, measured by spectral ellipsometry.

B. Calculation of $L^*a^*b^*$ Coordinates From RGB Values

The coordinate conversion is done in three following steps.

1) Conversion from RGB to sRGB [26]:

$R_{\mathrm{sRGB}} = (R/255)/12.92$ if $R/255 \leq 0.04045$

$R_{\mathrm{sRGB}} = ((R/255 + 0.055)/1.055)^{2.4}$ otherwise

The same formulae apply to G and B.

2) Conversion from sRGB to XYZ [26]:

$$\begin{pmatrix} X \\ Y \\ Z \end{pmatrix} = \begin{pmatrix} 0.4124 & 0.3576 & 0.1805 \\ 0.2126 & 0.7152 & 0.0722 \\ 0.0193 & 0.1192 & 0.9505 \end{pmatrix} \begin{pmatrix} R_{\mathrm{sRGB}} \\ G_{\mathrm{sRGB}} \\ B_{\mathrm{sRGB}} \end{pmatrix}$$

3) Conversion from XYZ to $L^*a^*b^*$ [24]:

$L^* = 116\, f(Y/Y_n) - 16$

$a^* = 500((f(X/X_n) - f(Y/Y_n))$

$b^* = 200((f(Y/Y_n) - f(Z/Z_n))$

with

$X_n = 0.9505$, $Y_n = 1$, $Z_n = 1.0888$ (values at the white point),

$f(X/X_n) = X^{1/3}$ if $X/X_n > (24/116)^3$,

$f(X/X_n) = 841/108(X/X_n) + 16/116$ if $X/X_n \leq (24/116)^3$.

The same formulae apply to Y and Z.

ACKNOWLEDGMENT

The authors would like to thank the Fraunhofer ISE colleagues Johannes Eisenlohr, Frank Ensslen, Andreas Wessels, Harald Lautenschlager, Martin Heinrich and Martin Wiese for helping with device processing and characterization.

REFERENCES

[1] T. E. Kuhn, C. Erban, M. Heinrich, J. Eisenlohr, F. Ensslen, and D. H. Neuhaus, "Review of technological design options for building integrated photovoltaics (BIPV)," *Energy Buildings*, vol. 231, 2021, Art. no. 110381.

[2] H. Lee and H.-J. Song, "Current status and perspective of colored photovoltaic modules," *WIREs Energy Environ.,* 2021, e403, doi: 10.1002/wene.403.

[3] T. Ameri *et al.*, "Fabrication, optical modeling, and color characterization of semi transparent bulk-heterojunction organic solar cells in an inverted structure," *Adv. Funct. Mater.*, vol. 20, no. 10, pp. 1592–1598, 2010.

[4] J. H. Noh, S. H. Im, J. H. Heo, T. N. Mandal, and S. I. Seok, "Chemical management for colorful, efficient, and stable inorganic-organic hybrid nanostructured solar cells," *Nano Lett.*, vol. 13, no. 4, pp. 1764–1769, 2013.

[5] S. G. Hashmi *et al.*, "Dye-sensitized solar cells with inkjet-printed dyes," *Energy Environ. Sci.*, vol. 9, no. 7, pp. 2453–2462, 2016.

[6] J. H. Selj, T. T. Mongstad, R. Søndenå, and E. S. Marstein, "Reduction of optical losses in colored solar cells with multilayer antireflection coatings," *Sol. Energy Mater. Sol. Cells*, vol. 95, no. 9, pp. 2576–2582, 2011.

[7] C. Kutter *et al.*, "Decorated building-integrated photovoltaic modules: Powerloss, color appearance and cost analysis," in *Proc. 35rd Eur. Photovolt. Sol. Energy Conf. Exhib.*, Brussels, Belgium, 2018, pp. 1488–1492.

[8] J. Escarré *et al.*, "When PV modules are becoming real building elements: White solar module, a revolution for BIPV," in *Proc. 42nd IEEE Photovolt. Specialists Conf.*, New Orleans, LA, USA, 2015, pp. 1–2.

[9] E. Klampaftis, D. Ross, G. Kocher-Oberlehner, and B. S. Richards, "Integration of color and graphical design for photovoltaic modules using luminescent materials," *IEEE J. Photovolt.*, vol. 5, no. 2, pp. 584–590, 2015.

[10] S. Mertin *et al.*, "Reactively sputtered coatings on architectural glazing for coloured active solar thermal façades," *Energy Buildings*, vol. 68, pp. 764–770, 2014.

[11] A. Schüler, M. Joly, and V. H. Le Caër, "Interference filter with angular independent orange colour of reflection and high solar transmittance, suitable for roof-integration of solar energy systems," Patent application, WO2014045144A1, 2014.

[12] O. Höhn, B. Bläsi, T. Kroyer, A. Hinsch, and T. Kuhn, "Glazing unit, process for their preparation and their use," Patent, DE102017203105B4, 2017.
[13] T. Starkey and P. Vukusic, "Light manipulation principles in biological photonic systems," *Nanophotonics*, vol. 2, no. 4, 2013.
[14] P. Vukusic and J. R. Sambles, "Shedding light on butterfly wings," in *Proc. SPIE*, San Diego, CA, USA, 2001, Art. no. 85, pp. 289–307.
[15] S. Kinoshita, S. Yoshioka, and K. Kawagoe, "Mechanisms of structural colour in the morpho butterfly: Cooperation of regularity and irregularity in an iridescent scale," *Proc. Roy. Soc. B, Biol. Sci.*, vol. 269, no. 1499, pp. 1417–1421, 2002.
[16] S. Kinoshita, S. Yoshioka, Y. Fujii, and N. Okamoto, "Photophysics of structural color in the morpho butterflies," *Forma*, vol. 17, pp. 103–121, 2002.
[17] W. Friedrich, P. Knipping, and M. Laue, "Interferenzerscheinungen bei röntgenstrahlen," *Ann. Phys.*, vol. 346, no. 10, pp. 971–988, 1913.
[18] H. A. Macleod, *Thin Film Optical Filters*. 3rd ed. Boca Raton, USA: Taylor & Francis, 2001.
[19] K. Chung *et al.*, "Flexible, angle-independent, structural color reflectors inspired by morphobutterfly wings," *Adv. Mater.*, vol. 24, no. 18, pp. 2375–2379, 2012.
[20] B. Bläsi, T. Kroyer, O. Höhn, C. Ferrara, and T. E. Kuhn, "Coloured module glass for BIPV inspired by morpho butterfly," in *Proc. OSA Light, Energy Environ. Congr.*, Leipzig, Germany, 2016, Paper PW5A.2.
[21] B. Bläsi *et al.*, "Morpho butterfly inspired coloured BIPV modules," in *Proc. 33rd Eur. Photovolt. Sol. Energy Conf. Exhib.*, Amsterdam, The Netherlands, 2017, pp. 2630–2634.
[22] D. Nečas and P. Klapetek, "Gwyddion: An open-source software for SPM data analysis," *Open Phys.*, vol. 10, no. 1, pp. 181–188, 2012.
[23] P. Baliozian *et al.*, "PERC-based shingled solar cells and modules at fraunhofer ISE," *Photovolt. Int.*, vol. 43, pp. 129–145, 2019.
[24] E. C. Carter *et al.*, *Colorimetry,* Technical report, 3rd ed. Vienna, Austria: CIE, Central Bureau, vol. 15, 2004.
[25] J. Eisenlohr *et al.*, "Highly efficient coloured BIPV modules with anti-glare properties," in *Advanced Building Skins*, Bern, Switzerland: Advanced Building Skins GmbH, Oct. 2018.
[26] *Multimedia Systems and Equipment - Colour Measurement and Management*, IEC 61966-2-1:1999, 1999.